Introduction

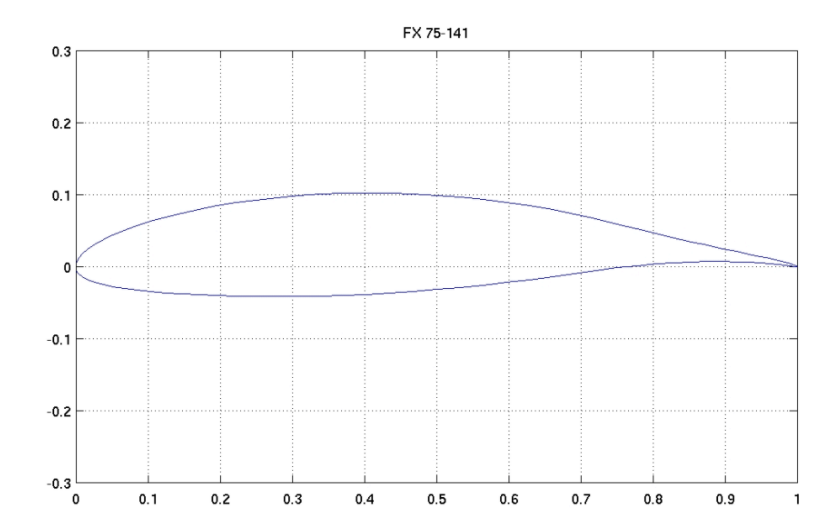
In order to keep costs low, computational methods are more commonly used, rather than wind tunnel and flight tests, to predict the performance and handling characteristics of aircraft. Of primary importance are the airfoil parameters. Therefore, it is of interest to establish a validation regime of computational methods for design and analytical purposes by comparing the results.

In this project, the flow pattern of the Wortmann FX 75-141 airfoil has been analysed on two-dimensional turbulent flow and computational fluid dynamic analysis has been implemented on the airfoil to find C_D and C_L values at different angles of attacks by using Siemens Star CCM+ 12.

Problem Statement

Wortmann FX 75-141 airfoil profile is used for the CFD analysis in this project. The Mach number is determined as M = 0.1457. Velocity of the flow is selected as 50 m/s. The total temperature of the free stream is estimated at 300 K, which is the same as the ambient temperature. For this Mach number, the flow is assumed as compressible. The dynamic viscosity is $\mu = 4.58 \times 10^{-5} \text{kg/m.s}$ and the density at the given temperature is $\rho = 1.177 \text{ kg/m3}$. The kinematic viscosity is calculated as $3.89 \times 10 \text{e-}5 \text{ m}^2 \text{ s}^{-1}$. The calculations has been performed for different angle of attacks starting from -6° to 18° by increasing the angle 2° for each trial.

Airfoil Geometry



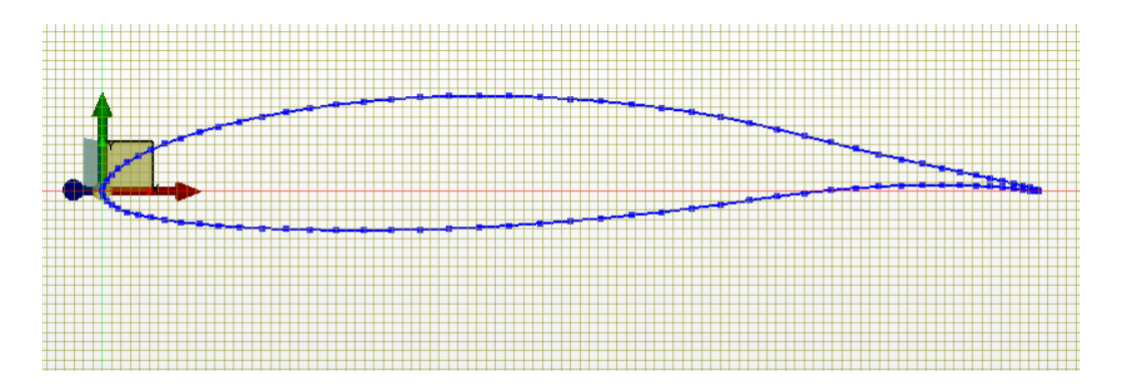


Fig.1 Airfoil Geometry of Wortmann FX 75-141

As it can be seen in the **Fig.1**, the point at front of the airfoil is a leading edge. The trailing edge is the minimum point of curvature at the rear side of the airfoil. The straight line which joins the leading edge and trailing edge of the airfoil profile is chord line. Chamber line is the location of the points at the midpoint between the upper and lower side of an airfoil. Grid shape selected as a square and grid spacing size is 0.01 m. Total length of the airfoil is selected as 1 m. The thickness of the airfoil is approximately estimated as 0.14 m.

Meshing

The meshes are generated by using the Star CCM+ 12 meshing tool and designed to fulfil the y + value requirement (0.1 < y + < 1). It comprises 15 prism layers with a 1.1 growth rate.

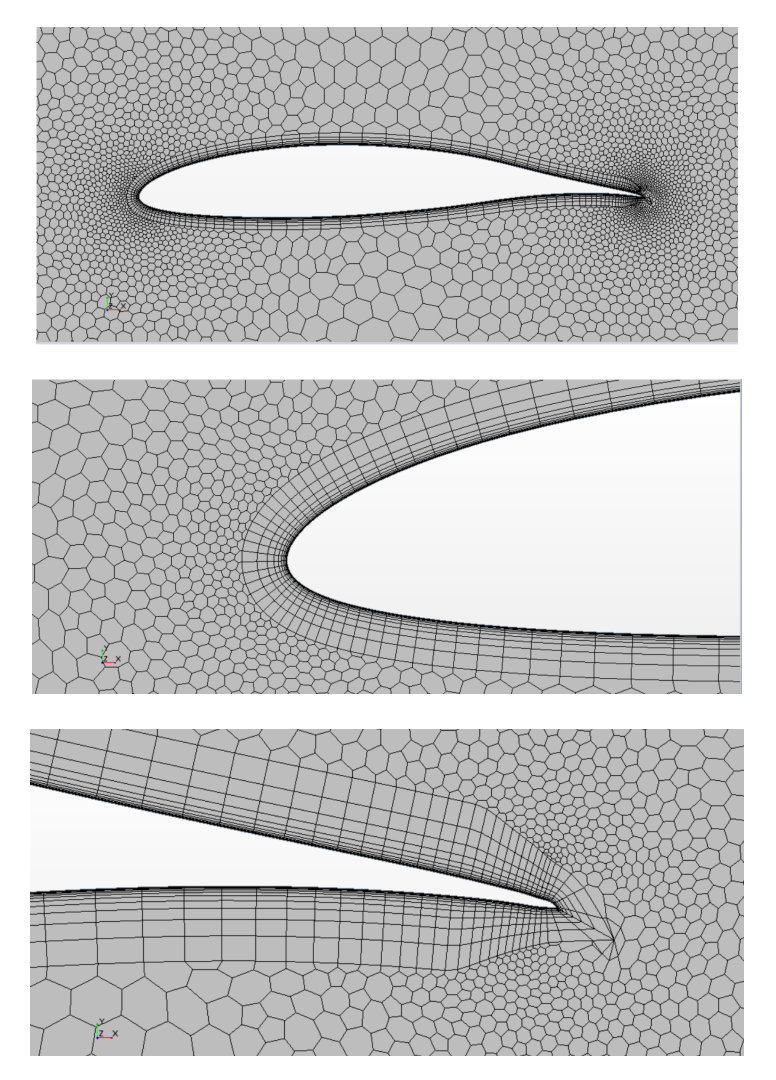


Figure 2 Airfoil Mesh Structure

Setting Up

The fluid, which is air, is compressible and the boundary conditions which are applied across the domain are shown in Figure 2 and defined in Table 1

Boundary Conditions

-Inlet

Velocity inlet with a magnitude depending on the Reynolds number

-Outlet

Static pressure outlet (Gauge pressure = 0 Pa)

-Symmetry Planes

Free slip stationary wall (Shear stress = 0 Pa)

- Symmetry Planes-2

Free slip stationary wall (Shear stress = 0 Pa)

-Airfoil

Non slip wall

Table 1: Conditions applied at the inlet boundary.

Reynolds number 6.5 e+6

Density 1.177 kg/m^3

Dynamic Viscosity 4.58E-5 Pa-s

Velocity V = 50 m/s

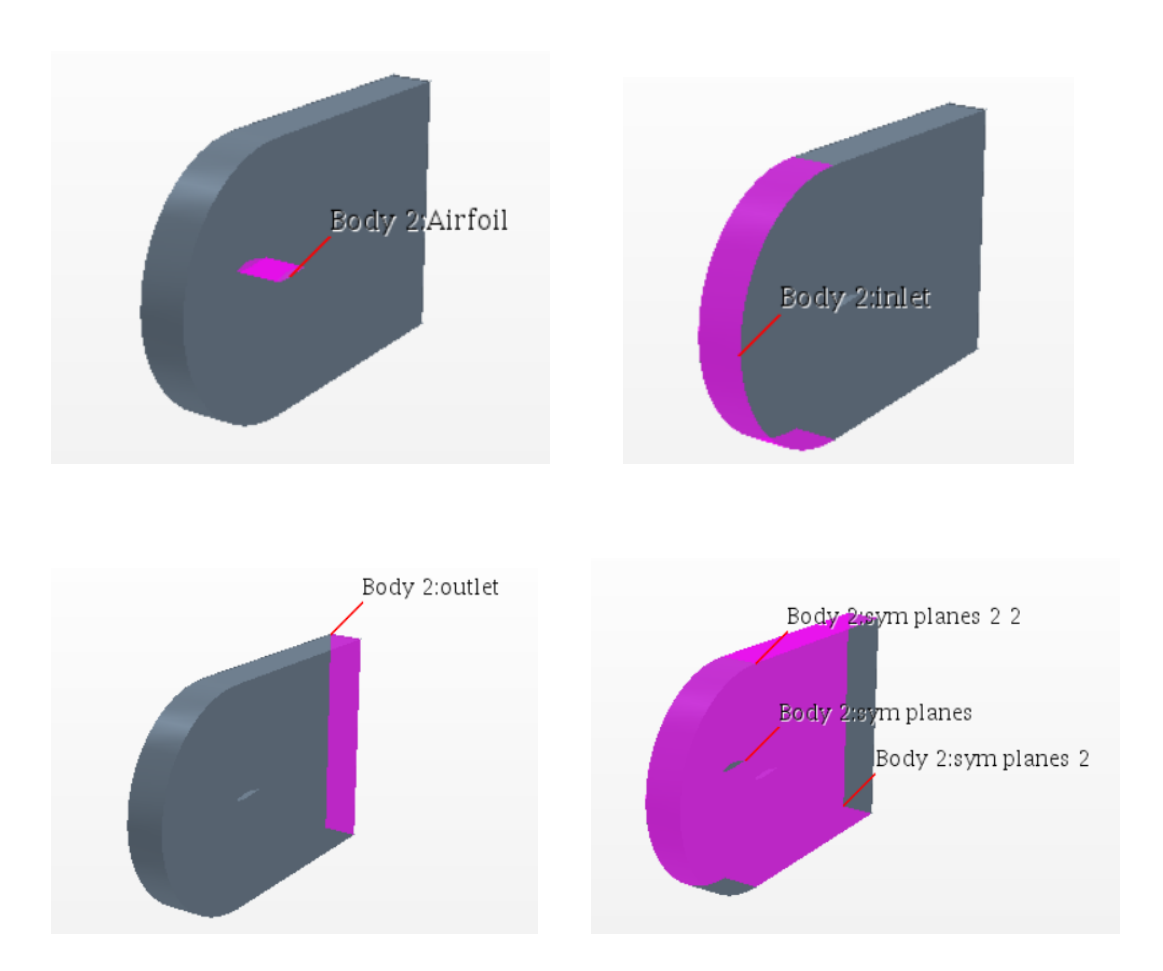


Figure 3 Schematic of the boundary conditions applied through the domain

Turbulence Model

Reynolds Averaged Navier-Stokes equations (RANS) and Standard Spalart-Allmaras Turbulence Model has been selected for this computational study. Generally, turbulence models strive to replace the genuine unstable Navier-Stokes equations by demonstrating mean and fluctuating quantities to generate Reynolds Averaged Navier-Stokes equations (RANS). Due to the statistical averaging procedure used to derive these equations, turbulence models based on RANS equations are known as statistical turbulence models.

Convergence

A convergent solution was obtained by considering a decrease towards the fourth decimal place in all the residuals of equations examined as a valid stopping criterion. Also, the power coefficients: C_L and C_D were followed and forced to obtain a constant trend by applying an additional criterion to ensure a limited accuracy of the fifth decimal place for the last 1000 iterations. In addition, a full multi-grid (FMG) initialization was realised to obtain an optimal initialization resulting in faster convergence.

Flow Separation

All durable objects moving in the fluid constitute viscous forces in the solid near-surface fluid layer acquiring a boundary fluid layer around them. Boundary layers can be laminar or turbulent. By calculating the Reynolds number of local flow conditions, we can decide whether the flow is laminar or turbulent. Flow separation occurs when the boundary layer commutes far enough against an unfavourable pressure gradient and at the same time the velocity of the boundary layer relative to the object descends to nearly zero. In aerodynamics, flow separation can frequently result in increased drag. Therefore, much effort and research has been put into the design of aerodynamic and hydrodynamic surfaces that delay flow separation and keep the local flow connected for as long as possible.

Two-Dimensional Results

Drag Coefficient

The results for the lift coefficient are given in the graph below. In Figure 4, it is observed that the drag force increases continuously in the analyses which are performed at different angles of attack ranging from -6 degrees to 18 degrees for the airfoil.

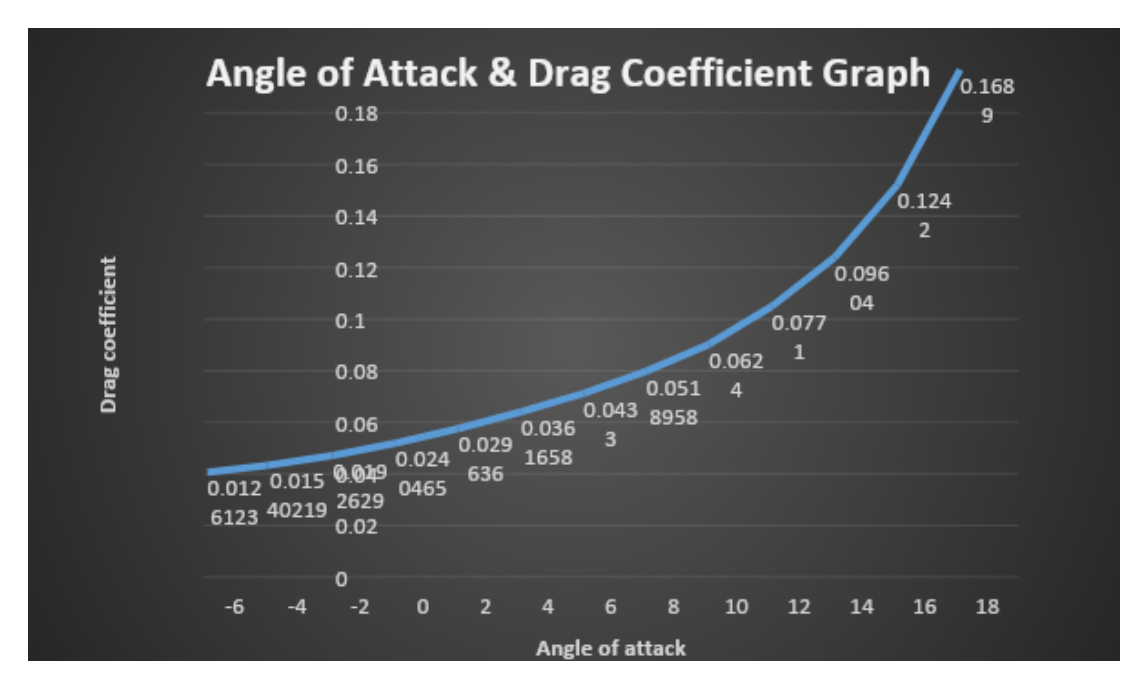


Figure 4

Lift Coefficient

In the experiments performed at different angles for the lifting force, it is observed that the lifting force increases continuously until the maximum lifting force is obtained at 14° angle. After that point, it is observed that the lift force starts to decrease, because the lift force required for the aircraft to take off is provided at that point.

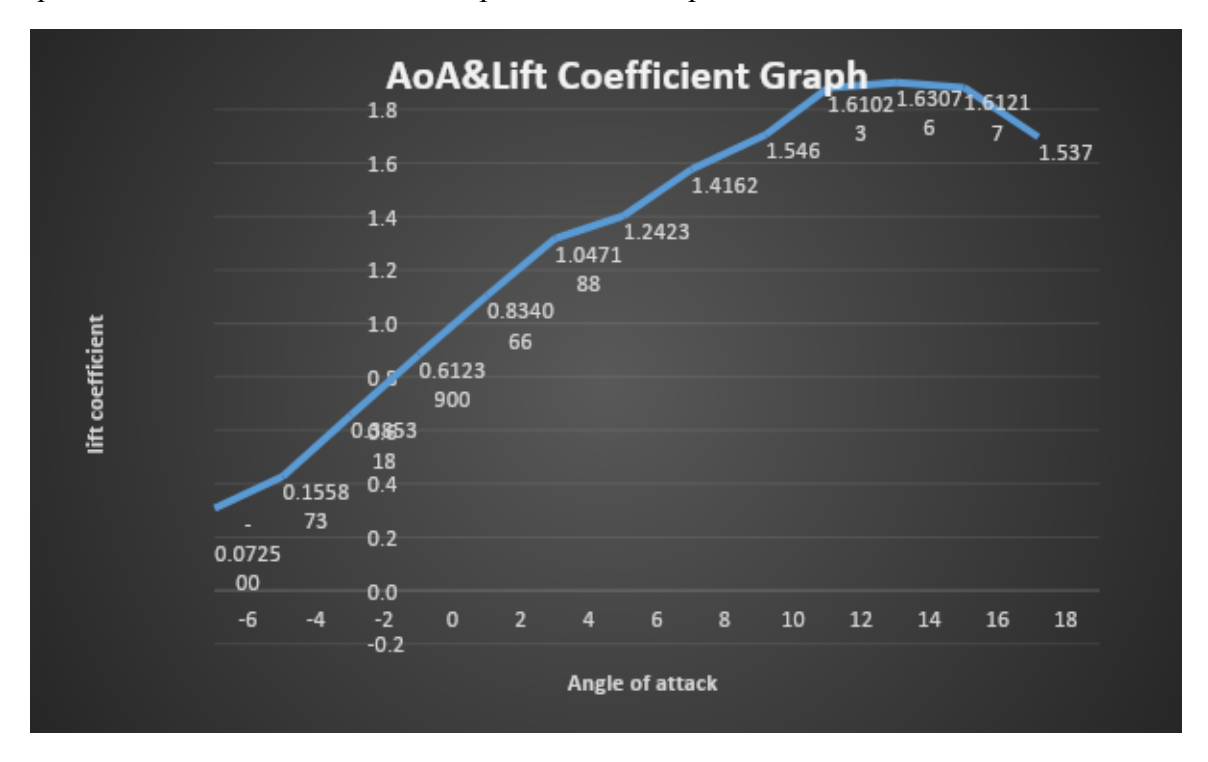


Figure 5

L/D Ratio & Angle of Attack Graph

As it can be seen in the L/D Ratio & AoA chart below; once the angle of attack is increased, the L/D ratio increases and when the angle of attack value is 4° , the maximum L/D ratio is obtained. After this, it can be observed in the graph below that the L/D ratio starts to decrease as the drag force starts to increase at 4° .

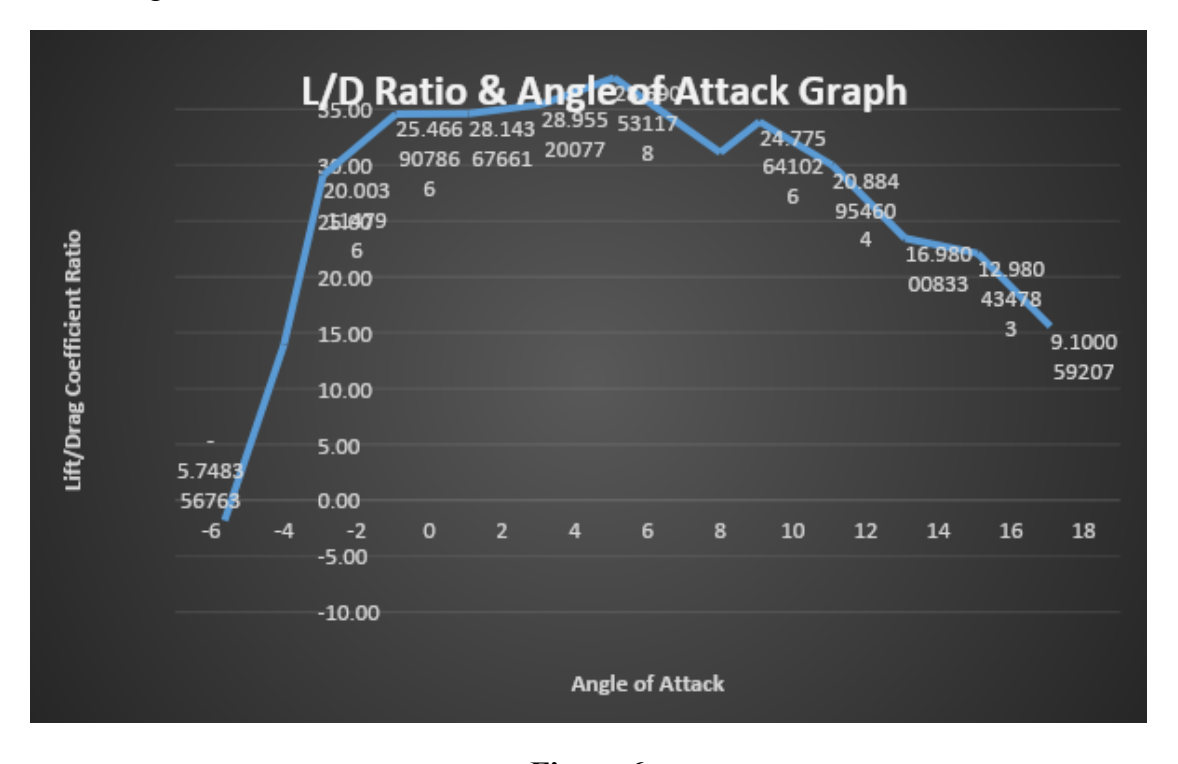


Figure 6

AoA	Drag Coefficient	Lift Coefficient	L/D Ratio
-6	0.0126123	-0.072500	-5.748356763
-4	0.01540219	0.155873	10.12018421
-2	0.0192629	0.385318	20.0031148
0	0.0240465	0.6123900	25.46690787
2	0.029636	0.834066	28.14367661
4	0.0361658	1.047188	28.95520077
6	0.0433	1.2423	28.69053118
8	0.0518958	1.4162	27.28929894
10	0.0624	1.546	24.77564103
12	0.0771	1.61023	20.8849546
14	0.09604	1.63076	16.98000833
16	0.1242	1.61217	12.98043478
18	0.1689	1.537	9.100059207

Table 1 Schematic Diagram of the Airfoil Profile According to Different Angles of Attack

Pressure Distribution

Below **figure 7 and 8** illustrates the pressure distribution on the upper and lower stream of air foil for 0° and 14° angle of attack subsequently. Pressure difference between upper and lower region of the airfoil is greater in Fig. 7 than Figure 8. During the flight, the pressure difference is at the highest level which creates lift force to keep the aircraft up on air. The value of lift coefficient is maximum at this angle of attack 14°. Maximum lift is obtained due to maximum pressure difference on the upper and lower surface of the airfoil.

It is observed in **Figure 9** and **Figure 10** that when the angle of attack increases, the pressure difference in the lower region of the airfoil also increases, this increasing pressure also create the increase in the lift force and allows the aircraft to take off at 14°. Once the angle of attack is increased, the pressure and pressure coefficient is also decreased in the upper region of the airfoil at the same time automatically. These pressure differences create lifting force to enable the aircraft to take off.

Furthermore, it is also observed that from **Figure 12 and 13** when the angle of attack is at 0°, pressure and pressure coefficient differences between upper and lower stream of the airfoil are at the highest value. Because the aircraft continues to fly in the air and this maximum pressure difference allows the aircraft to stay in the air and accelerate. When the aircraft starts to descend downwards, this pressure difference will decrease with the opening of the flaps and with the decrease of this pressure difference, the aircraft will start to move downwards gradually with the control of the autopilot or pilot.

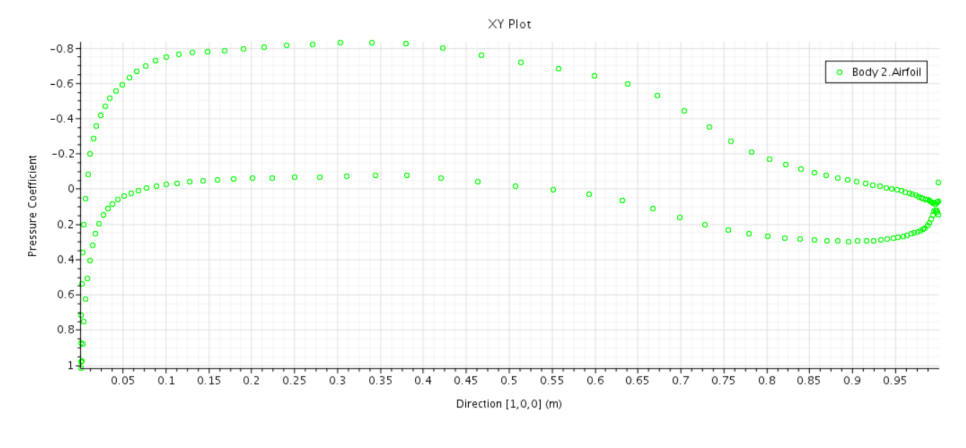


Figure 7 Angle of Attack at 0

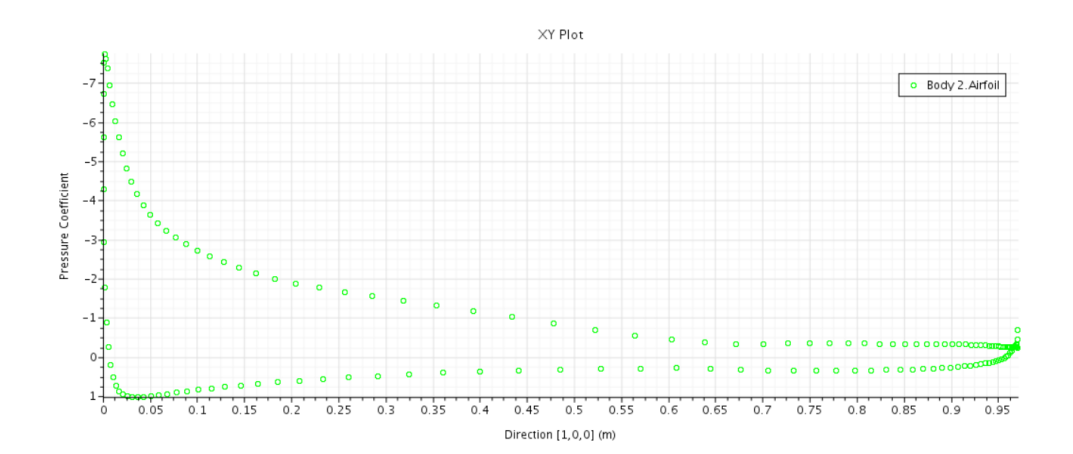


Figure 8 Angle of Attack at 14⁰

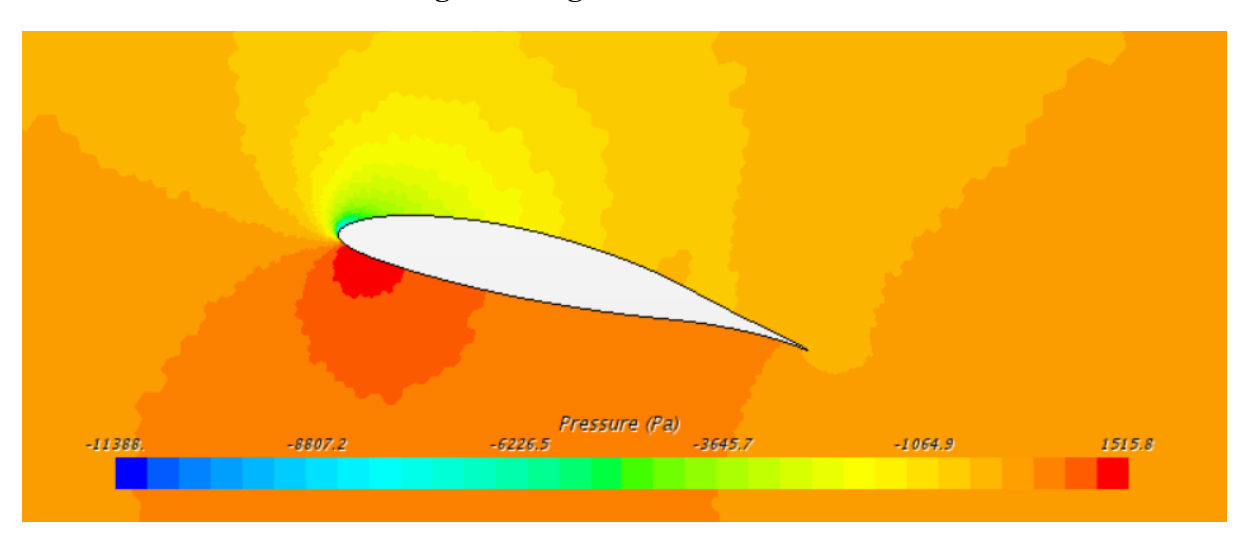


Figure 10 Angle of Attack at 14⁰

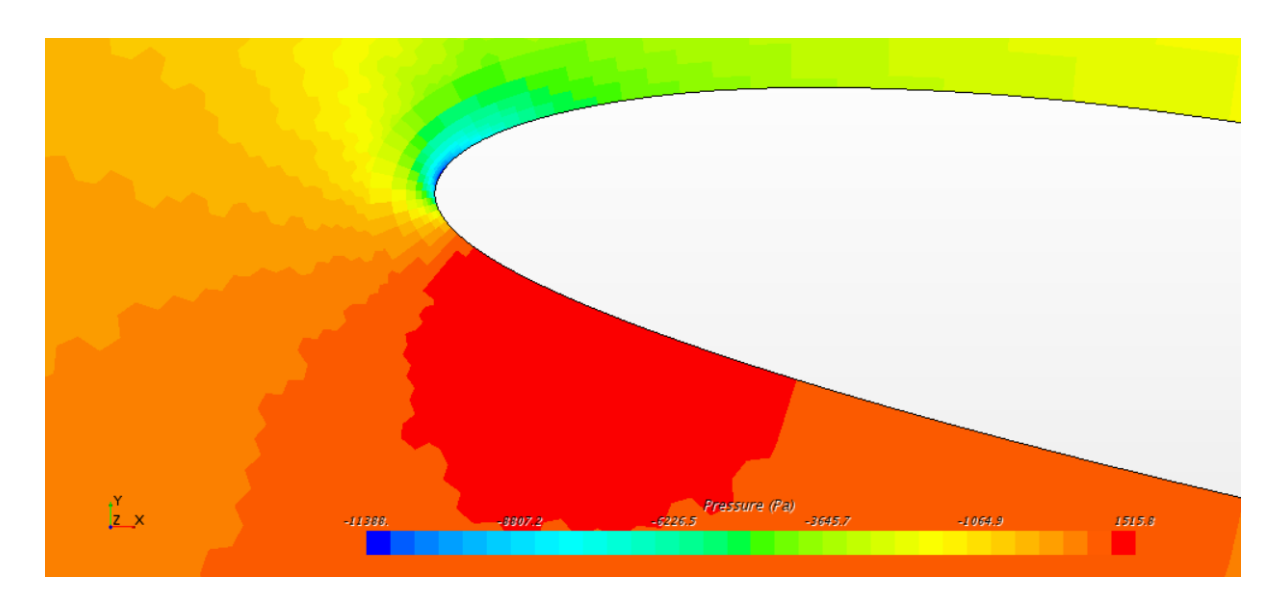


Figure 11 Angle of Attack at 14⁰

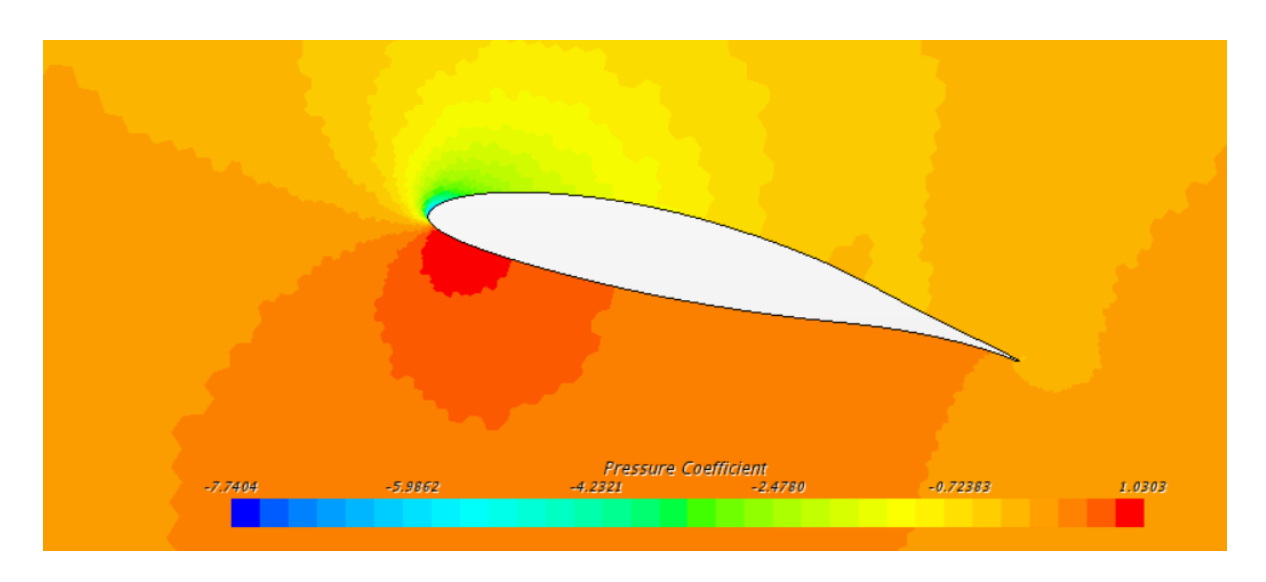


Figure 12 Angle of Attack at 14⁰

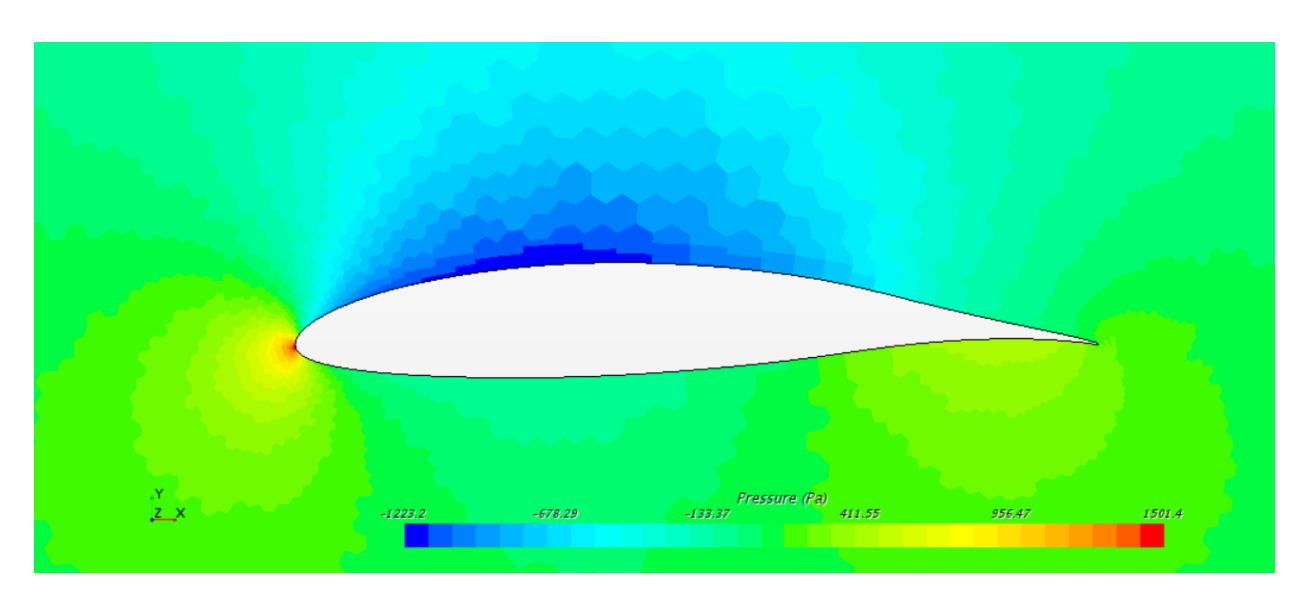


Figure 13 Angle of Attack at 0^0

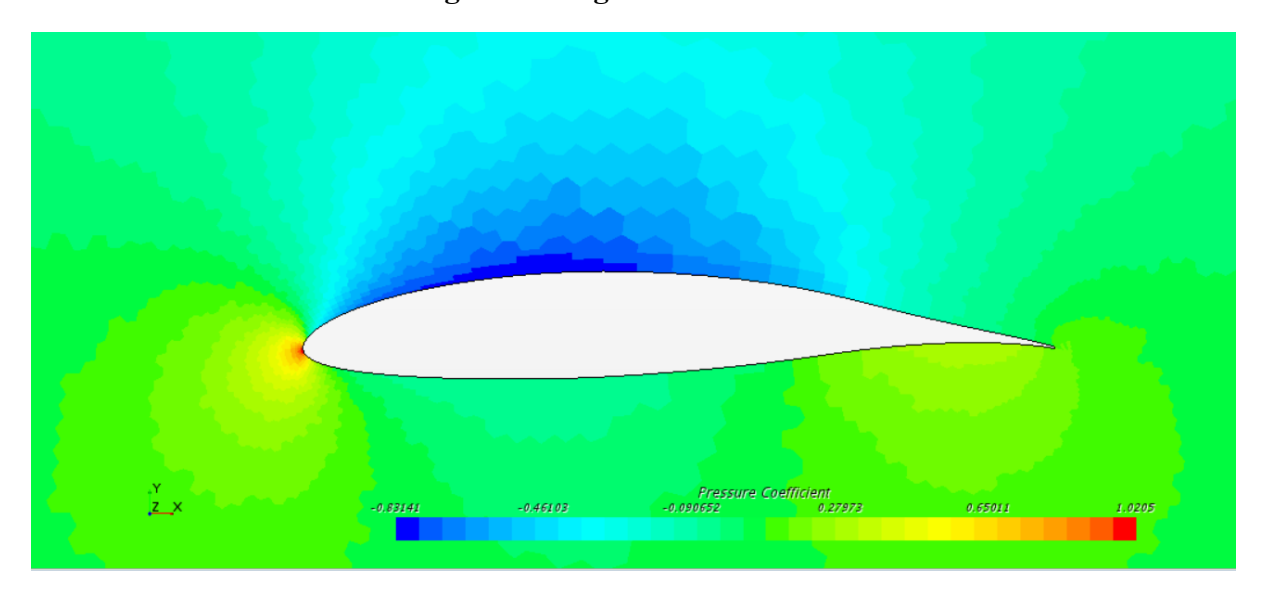


Figure 14 Angle of Attack at 0^0

Velocity Profile

In the graphic below, it is observed that the velocity changes obtained at 0° and 14° attack angles. Once the attack angle is applied at 14°, it is seen that the velocity difference between the lower and upper regions of the airfoil surfaces increase due to the increase in drag force. In the upper zone of the airfoil: the higher speed, the lower pressure; in the lower zone: the low speed allows the pressure value to increase and enable to form sufficient lifting force to lift the aircraft up.

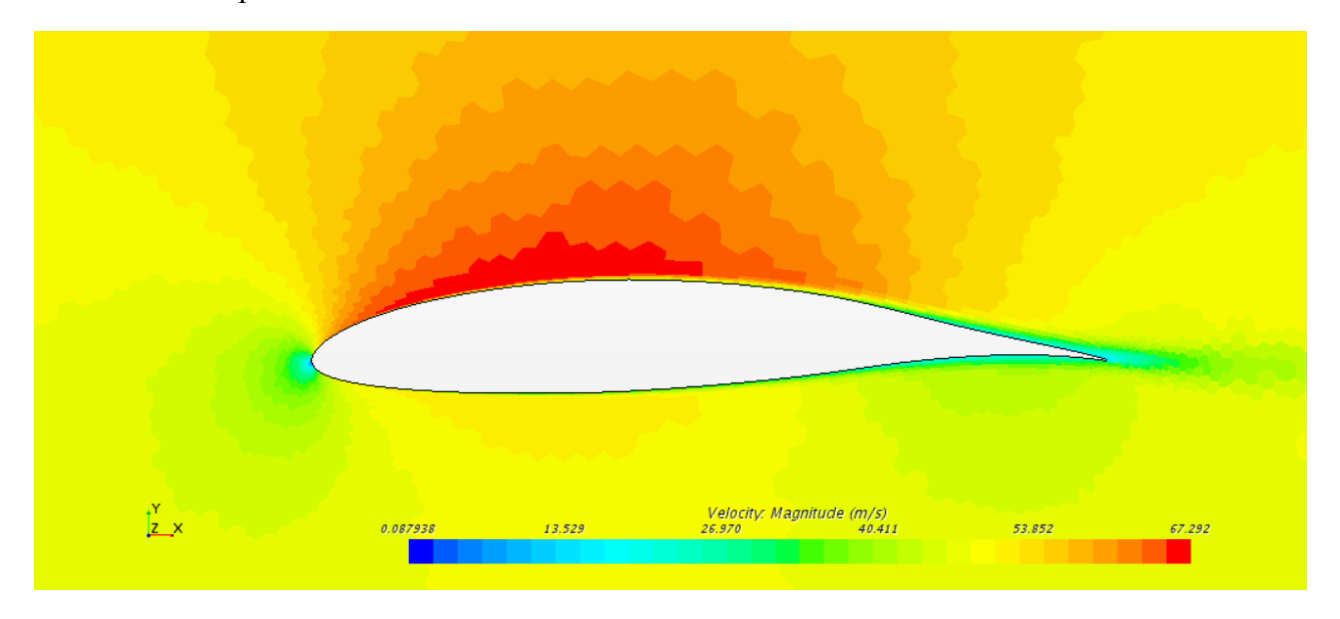


Figure 15 Angle of Attack at 0^0

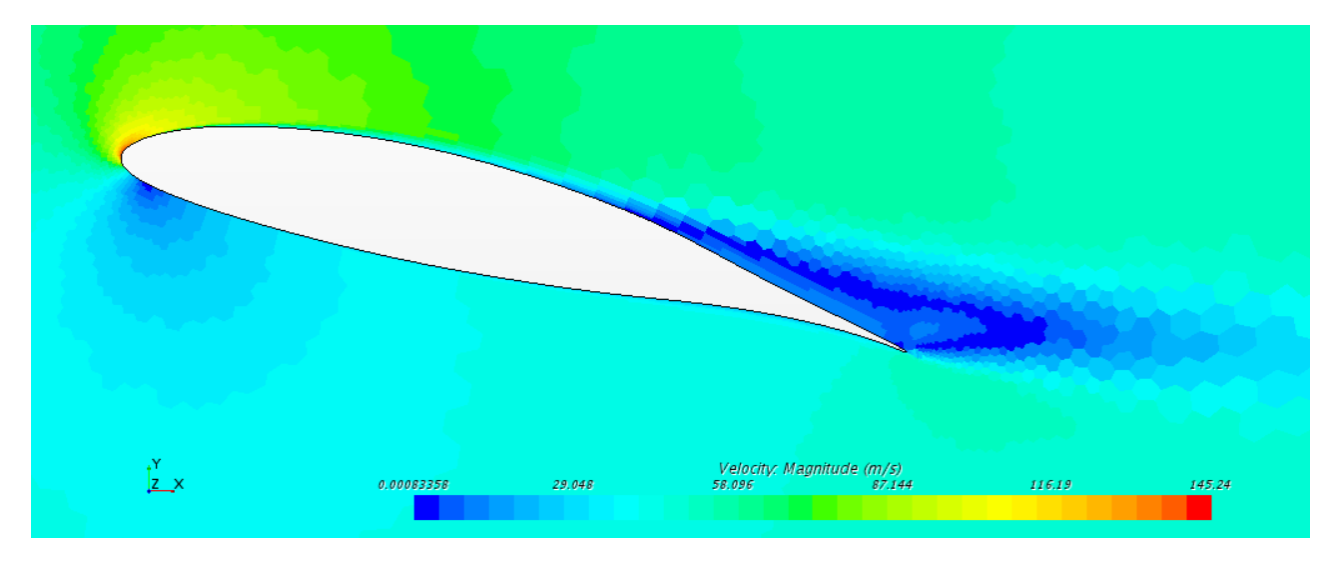


Figure 16 Angle of Attack at 14⁰

Flow Separation

The separation of the boundary layer leads to changes in the pressure distribution around the airfoil. As shown in **Figure 16** above, the separated flow has much greater pressure distribution at the top of the airfoil. This causes the airfoil to have less lift as the flow is separated. Also, in the tail section of the airfoil, the separated flow has much less pressure distribution. The horizontal component of that distribution causes the airfoil to have a much greater drag component. Therefore, the separation of the boundary layer causes the airfoil to have a drastic loss in lift which causes stall, and a major increase in drag.

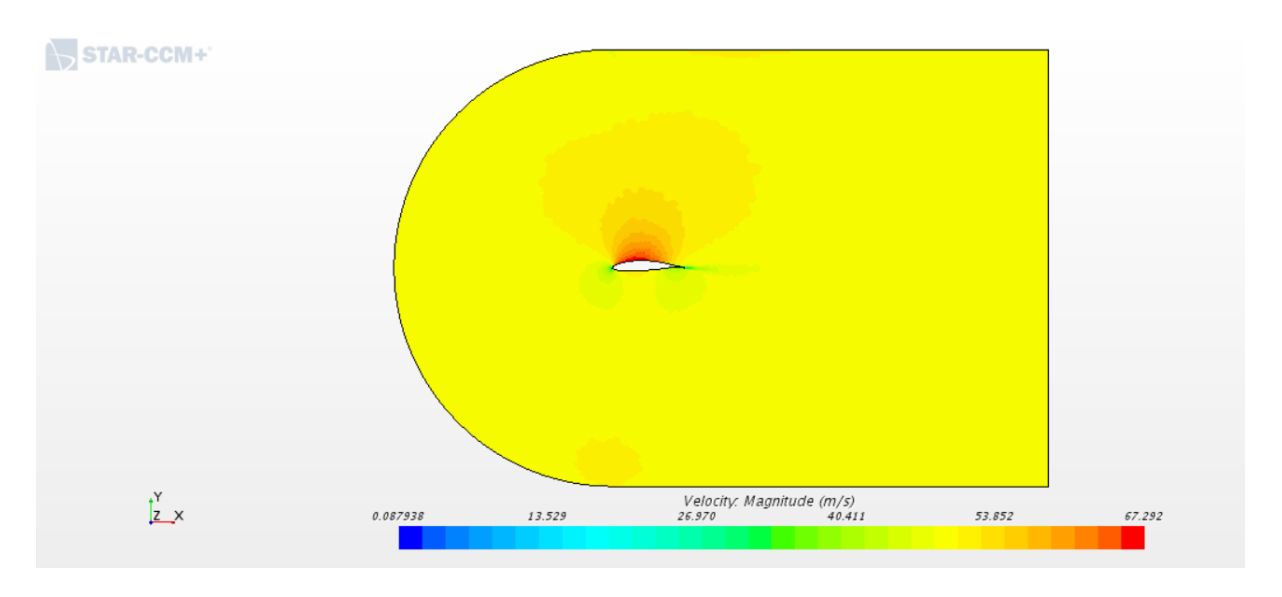


Figure 17 Angle of Attack at 0^0

Drag Coefficient

As it can be seen in the drag coefficient curve below, it is observed that the drag coefficient increases when we increase the angle of attack, and there is a time delay reaching the drag coefficient value towards 0 because of the increasing angle of attack. During the flight time, drag coefficient is settled to 0.096 at 14°, but drag coefficient is settled to 0.024 at 0°

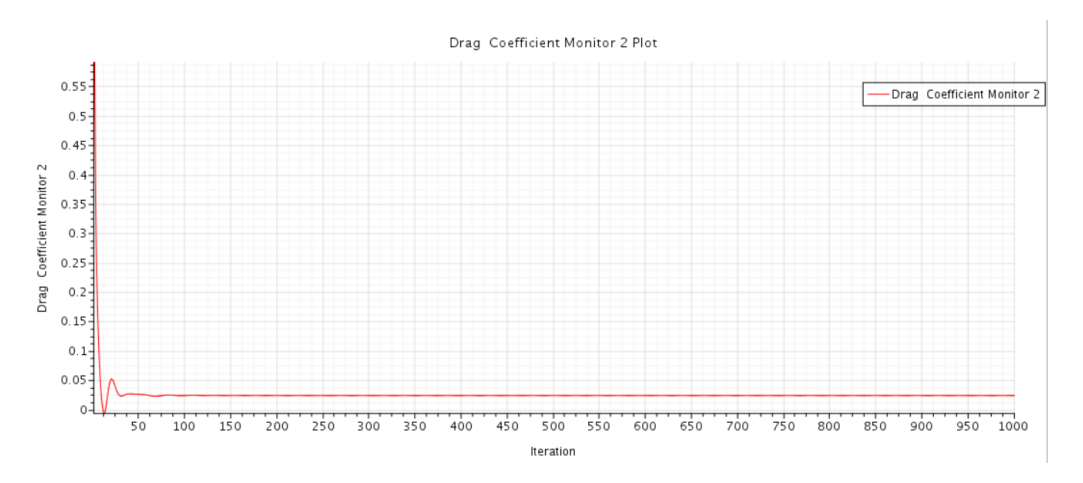


Figure 18 AoA at 0°

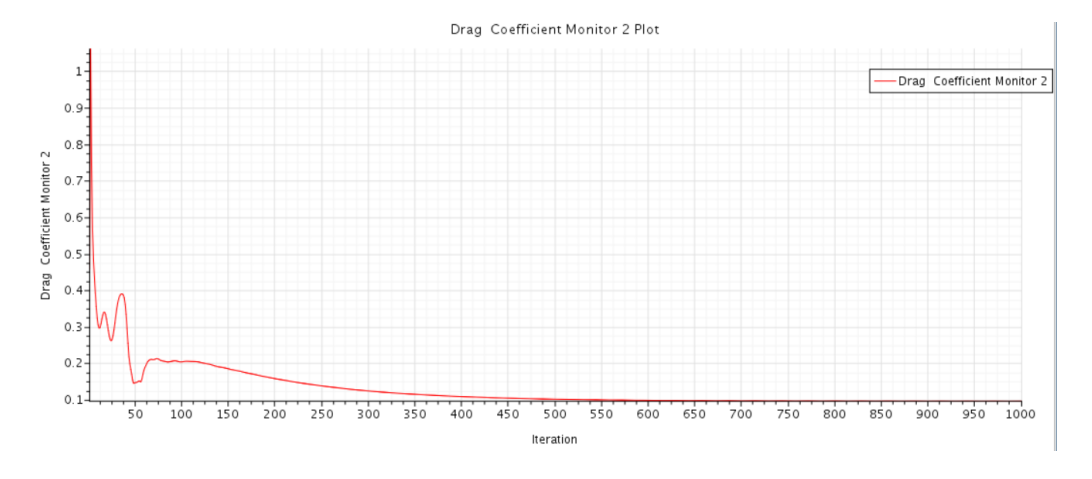


Figure 19 AoA at 14°

Lift Coefficient

As seen in the Figure 18 and 19, The greater value of the angle of attack at 14° , the upper surface flow is separated and the lower lift coefficient is obtained after that angle. Because max. lift is obtained at that angle.

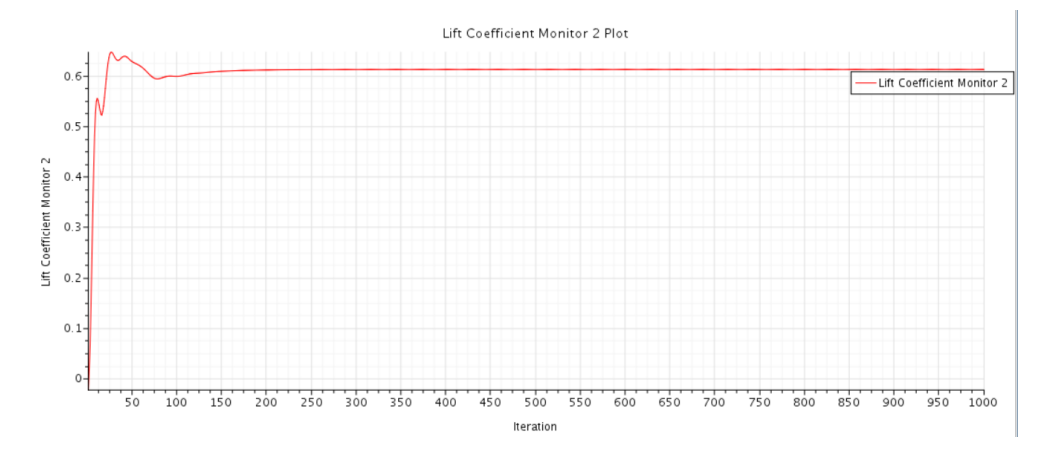


Figure 20 AoA at 0°



Figure 21 AoA at 14°

Residual Forces

It is observed that when the angle of attack is increased, the residual forces also increase.

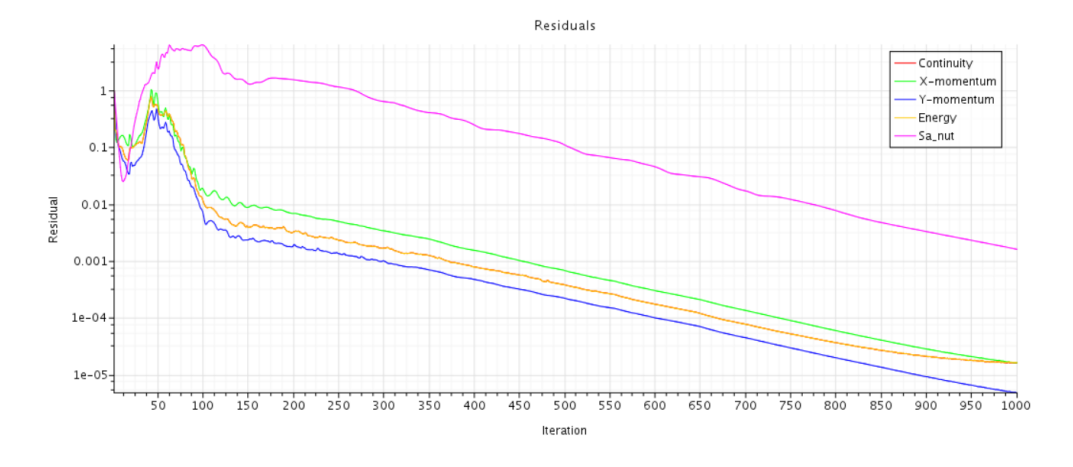


Figure 22 AoA at 14°

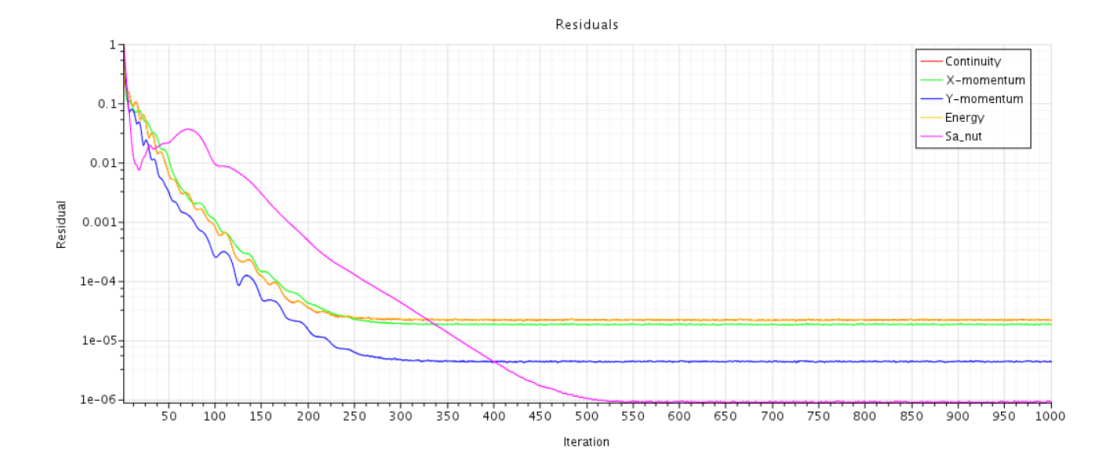


Figure 23 AoA at 0°

DISCUSSION & CONCLUSION:

In this computational study, the airfoil profile has been used to analytically predict lift and drag coefficients for Wortmann FX75-141 airfoil. Siemens Star CCM+ 12 has been used within a workbench project to compute the transonic, compressible flow over a Wortmann FX-75 141 airfoil. The aim of this study is to understand the flow pattern over an airfoil of Wortmann FX-75 141 type aircraft and the analysis of airfoil speed, drag, lift, pressure coefficient and residual forces parameters using CFD. As a result of this study, it is assumed that CFD Analysis will continue to contribute significantly to the comprehension of the flow pattern over an airfoil. Different type of airfoil profiles can be studied and analysed by referencing this study for further investigation and comparison. The following are fundamental results obtained from the studies carried out in the present study.

- 1. For an airfoil with chord length 1 m, the coefficient of lift increases from -0.0725 for 0° to 1.63076 for 14° angles of attack and again decreases to 1.537 for 18°.
- 2. The maximum value of lift coefficient is obtained at the stall angle.
- 3. After the stall angle, the flow separation takes place away from the trailing edge which diminishes the lift generated.